Kinesin's Neck-Linker Determines its Ability to Navigate Obstacles on the Microtubule Surface

Gregory J. Hoeprich[1], Andrew R. Thompson[1], Derrick P. McVicker[2], William O. Hancock[3] and Christopher L. Berger[1,2]

[1]Department of Molecular Physiology & Biophysics, and [2]Cell and Molecular Biology Program, University of Vermont, Burlington, VT 05405; [3]Department of Bioengineering, Pennsylvania State University, University Park, PA 16802

SUPPORTING MATERIAL

Determining the Rate of Kinesin Photobleaching

To determine the bleaching time of the dual eGFP tagged kinesin constructs, we strongly bound kinesin-2 to paclitaxel microtubules with AMP-PNP, a non-hydrolyzable analog of ATP that mimics the strongly bound ATP nucleotide state. Samples were prepared exactly as if performing a single molecule motility assay except 1mM ATP was replaced with 1mM AMP-PNP.

Data was analyzed by generating kymographs of microtubules with the MultipleKymograph plug-in for ImageJ software, version 1.46r (National Institutes of Health, Bethesda, MD) and the duration of emitted light from the eGFP tag on the kinesin constructs was measured. A cumulative frequency plot was generated and fit with $C(x) = 1 - e^{\frac{x}{x_0}}$, where x_0 represents the average bleaching time (Fig. S1).

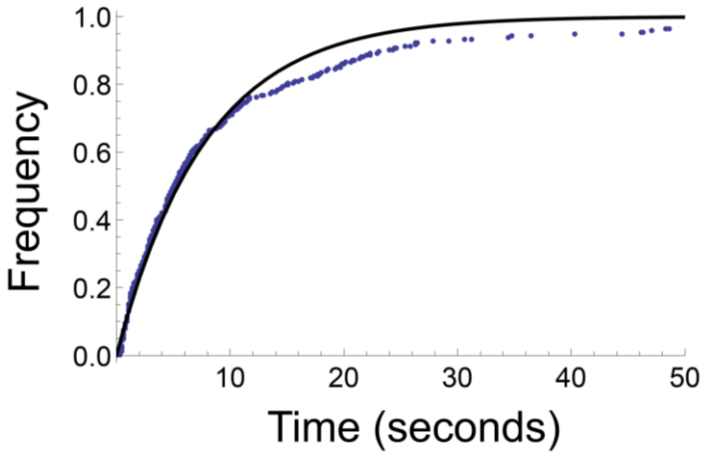

FIGURE S1 Cumulative frequency plot (black curve) of kinesin-2 eGFP photobleaching events (blue dots), where the average photobleaching time was 7.8 ± 1.5 s. Kinesin-2 was diluted to single molecule concentrations and then incubated with 1mM AMP-PNP and pipetted into the flow cell in a manner identical to that used in the motility assays. The theoretical distance the kinesin constructs could move before photobleaching was an average of 4.5 times farther than their observed characteristic run lengths as calculated below:

$$\left(\frac{\text{velocity of kinesin}\left(\frac{\text{nm}}{\text{s}}\right)*\text{bleaching time (s)}}{\text{Characteristic Run Length(nm)}}\right).$$

Histograms for Kinesin Pausing Data

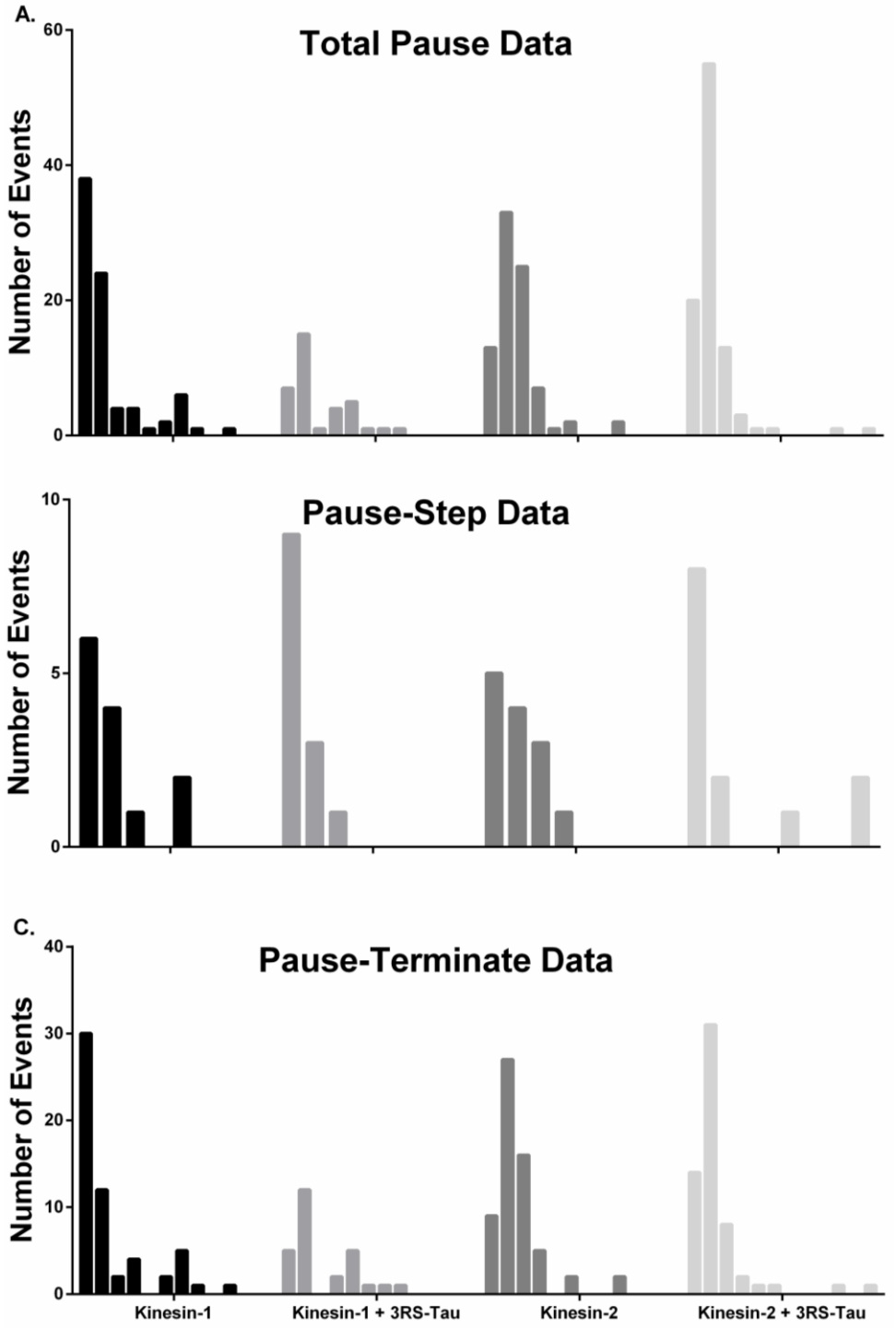

FIGURE S2 Histograms for kinesin-1 and kinesin-2 pausing data in the absence and presence of 3RS-Tau. (A) Histograms of total pause data, (B) pause-step data, and (C) pause-terminate data. The x-axis represents time, where the bin width is 2 seconds for every kinesin/Tau condition.

Discussion of 3RS-Tau and Density of 3RS-Tau on the Microtubule Surface

Tau has previously been shown to be either static or diffusing on the microtubule surface (1) (2). 3RS-Tau has more stationary events (78%) than diffusive compared to 4RL-Tau (55%) and resides longer on the lattice, 21.6 s versus 6.2 s, respectively (2). The shift between these two states may be regulated by phosphorylation as modification at the N-terminus of Tau increases the diffusive events seen *in vitro* (unpublished data). Post-translational modifications such as these may help regulate Tau's static-to-diffusive behavior and its ability to inhibit kinesin-1 motility *in vivo*, an interesting future direction to explore.

3RS-Tau was selected over 4RL-Tau for the analyses below as it has a higher ratio of static to diffusive events, has a longer dwell time on the microtubule surface as seen *in vitro*, and acts as a better inhibitor of kinesin motility (2). To calculate the number of Tau per unit length of microtubules, we prepared 3RS-Tau decorated microtubules, as if performing a single molecule motility assay, but without kinesin present (see *Materials and Methods*). Stabilized microtubules were incubated with 3RS-Tau at a ratio of 1:5 Tau to tubulin, where the ratio of Alexa 546-labeled 3RS-Tau to unlabeled 3RS-Tau was 1:600 to facilitate the imaging of individual Tau molecules at a final concentration of 300 nM total 3RS-Tau. Microtubules (1 µM) were imaged by TIRF microscopy as described above for the single molecule motility assay except that the acquisition rate was 10 frames / second for 100 seconds.

Data were analyzed by generating kymographs with MultipleKymograph plug-in for ImageJ software, version 1.46r (National Institutes of Health, Bethesda, MD). The number of labeled Tau molecules along the microtubules were counted at 4 different time points along the kymograph (t_0, t_{25}, t_{50} and t_{75} seconds) during a 100 second movie, where 38 microtubules were analyzed totaling 112 labeled Tau events. The total Tau (labeled Tau plus unlabeled Tau) was calculated per kinesin step for a 13 protofilament microtubule:

$$\frac{(\#\text{ of labeled Tau})(600\text{ fold excess unlabeled Tau})}{(\text{unit length of microtubule (nm)})} * \left(\frac{8\text{ nm}}{1\text{ kinesin step}}\right) * \left(\frac{1}{13\text{ protofilmaents}}\right).$$

The four time points were averaged and a final value of 2.03 x 10^{-2} Tau / kinesin step / protofilament (or 49.33 steps / Tau / protofilament) along a single protofilament. Additionally, it was calculated, per unit length of microtubule, one Tau molecule per 30 nm. (Note: Tau binds non-uniformly along the microtubule surface (Movies S2 and S4), but, for simplicity to find an estimated average value for Tau decoration, our analysis assumes an even distribution along the microtubule surface.)

Calculating Kinesin-1 and Kinesin-2's Stepping Probability

The Worm-Like Chain Model was used to model the neck-linkers non-linear force-extension relationship (3-5):

$$F(x) = \frac{K_B T}{p}\left(\frac{1}{4}\left(1 - \frac{x}{L}\right)^{-2} - \frac{1}{4} + \frac{x}{L}\right)$$

where K_B is Boltzmann's Constant, T is absolute temperature, p is the persistence length and L is the contour length. We used three different persistence lengths for calculating the stepping probability: 1nm, 1.2nm and 1.4nm as this was determined to be an acceptable range (**Table S1**)

(5). The contour lengths of the kinesin neck-linkers were calculated by multiplying the number of amino acids by 0.365 nm / residue (6) and then by 2 as there are two neck-linkers per kinesin. Each cis-proline present shortens the neck-linker by 0.548 nm (7). Neck-linker contour lengths, L:

kinesin-1: $\left(14 \text{ amino acids} * 0.365 \frac{\text{nm}}{\text{amino acid}}\right) 2 = 10.22 \text{ nm}$

kif3A/A: $\left(17 \text{ amino acids} * 0.365 \frac{\text{nm}}{\text{amino acid}} - 0.548 \frac{\text{nm}}{\text{proline}} * 1\text{proline}\right) 2 = 11.31 \text{ nm}$

kif3A/B: $\left(17 \text{ amino acids} * 0.365 \frac{\text{nm}}{\text{amino acid}} - 0.548 \frac{\text{nm}}{\text{proline}} * 1.5\text{proline}\right) 2 = 10.77 \text{ nm}$

The elastic energy stored within the two neck-linkers is: $E_i = \int_0^x F(x)dx$

The probability, q_i, for kinesin reaching a possible binding site (out of a possible five sites) on the microtubule lattice as well as the kinesin binding site distances were obtained from (8, 9). The values were calculated by: $q_i = \left(\sum_k \frac{q_k}{q_i}\right)^{-1}$ where $\frac{q_k}{q_i} = e^{-\left(\frac{E_k - E_i}{K_B T}\right)}$ (9). The start of the diffusional search of the kinesin front head was 4 nm in the plus-end direction and 0.5 nm to the left (10). All calculations were completed in MATLAB version R2012b (The MathWorks, Natick, MA).

TABLE S1 Probability of Kinesins Side-Stepping as a Function of Neck-Linker Contour Length with Different Persistence Lengths

	p (nm)	Front (F)	Left (L)	Front-Left (F-L)	Front-Right (F-R)	Right (R)
Kinesin-1	1	99.86	0.14	2.47E-04	5.06E-05	7.57E-11
	1.2	99.59	0.41	2.12E-03	5.65E-04	7.91E-09
	1.4	99.09	0.90	9.79E-03	3.16E-03	2.18E-07
Kinesin-2 (Kif3A/A)	1	98.96	1.00	2.69E-02	1.18E-02	2.53E-05
	1.2	97.72	2.12	1.00E-01	5.25E-02	3.14E-04
	1.4	95.97	3.60	2.70E-01	1.50E-01	1.88E-03
Kinesin-2 (Kif 3A/B)	1	99.55	0.44	4.24E-03	1.40E-03	2.41E-07
	1.2	98.89	1.08	2.25E-02	8.97E-03	6.53E-06
	1.4	97.85	2.04	7.39E-02	3.36E-02	6.85E-05

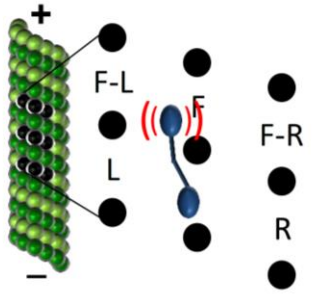

Percent probabilities of kinesin-1 and kinesin-2's front head binding to available microtubule binding sites using three different persistence lengths (p) for the neck-linkers (5). Kinesin-2, for each persistence length, has a higher probability of stepping off its protofilament counterclockwise compared to kinesin-1 during its diffusional search (shown in red brackets). (Animation is not drawn to scale and is for visual effect.)

Stochastic Modeling of Tau Inhibition

3RS-Tau-decorated microtubule tracks were simulated in Mathematica (Version 9, Wolfram Research) by generating large, two-dimensional sparse arrays (i.e. arrays containing mostly 0-valued cells) with an x-axis representing 8-nm steps along a microtubule protofilament and a y-axis corresponding to the length of time between each step, which effectively represents a kymograph. The y-axis of each array was scaled according to the mean velocity of the motor of interest, thus enabling all motility to occur along diagonal elements of the array. The array was

stochastically populated with 3RS-Tau (1-valued cells), characterized by an exponentially distributed dwell time (mean value = 21.6 s (2)) and an on-rate calculated as follows: we assumed that the presence of Tau as a 1:1 steric blocker effectively shortens the microtubule track length distribution, characterized by a parameter we denote as L_{eff}. Based on our previous work relating the observed microtubule track length distribution (L_o) and the observed characteristic run length ($X_{observed}$) (11), the distance that kinesin would be expected to move ($X_{expected}$) along the microtubule surface in the presence of Tau is given by:

$$X_{expected} = X_{observed}\left(1 - \frac{X_{observed}(L_{eff} + 2X_{observed})}{2(L_{eff} + X_{observed})^2}\right)$$

A landing rate of $4x10^{-6}$ $nm^{-1}s^{-1}$ was found to produce a L_{eff} value consistent with the observed effect of 3RS-Tau on kinesin-1 motility (Fig. S3).

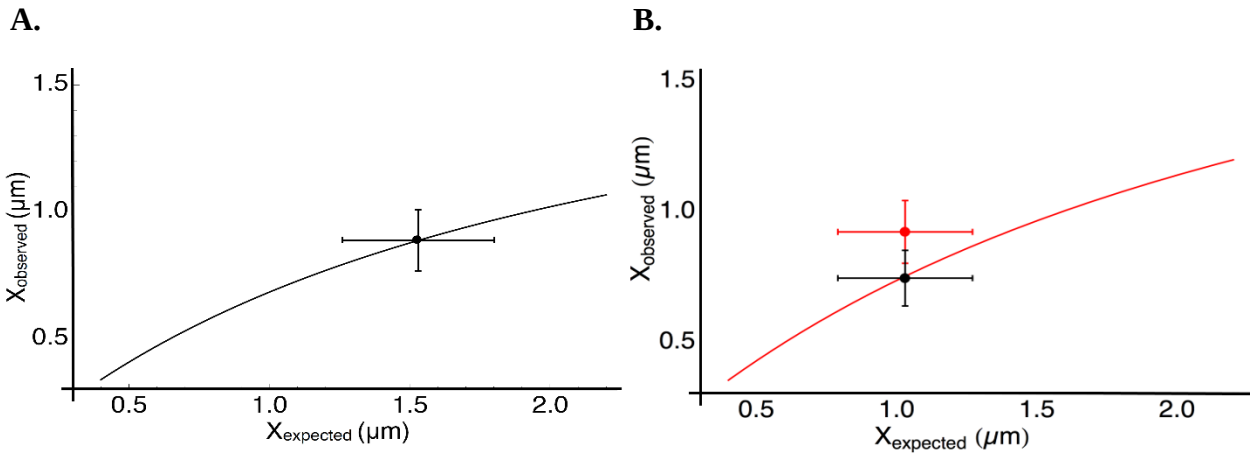

FIGURE S3 Model calibration using the observed 3RS-Tau inhibition of kinesin-1 and demonstrating kinesin-2 is able to navigate Tau obstacles. (A) The kinesin-1 characteristic run length in the absence of 3RS-Tau ($X_{expected}$) and the observed behavior in the presence of 3RS-Tau and track distribution effects ($X_{observed}$) (black dot) was used to calibrate the appropriate 3RS-Tau on-rate to yield agreement between the simulation of 1:1 3RS-Tau inhibition for kinesin-1 (black curve) over the range of potential $X_{expected}$ values. (B) Experimental data for kinesin-2 (red dot) show significant deviation from the simulated behavior if 3RS-Tau acted as a 1:1 inhibitor (red curve). Utilizing the simulation curve and the experimental $X_{expected}$ value for kinesin-2, a predicted value for $X_{observed}$ obeying the simulation results (black dot) was generated with an equal number of points (N=325, Table 1) to account for sampling uncertainty. This predicted value, $X_{observed}$, was found to be statistically significant from the experimental value (p-value = 5 X 10^{-3}) via permutation resampling (11), indicating that kinesin-2 both encounters 3RS-Tau in these experimental conditions and is able to bypass it. Error bars represent the 99% confidence intervals for the respective datasets.

Simulated motility experiments were performed by stochastically selecting a starting point on the array, followed by selection of both a motility event, a microtubule track length and a track landing point from the experientially derived run length and track length distributions as described previously (11). After adjusting the motility event length for any track termination effects, the motility event length was used to sample a diagonal strip of the matrix. If the sampled strip was empty (full of zeros), the run length was un-changed. If the strip contained a 1-value (due to the presence of a 3RS-Tau), the run length was adjusted to the number of steps preceding the 3RS-Tau site. Periodic boundary conditions were implemented to prevent motility events from being terminated by the edges of the array (Fig. S4).

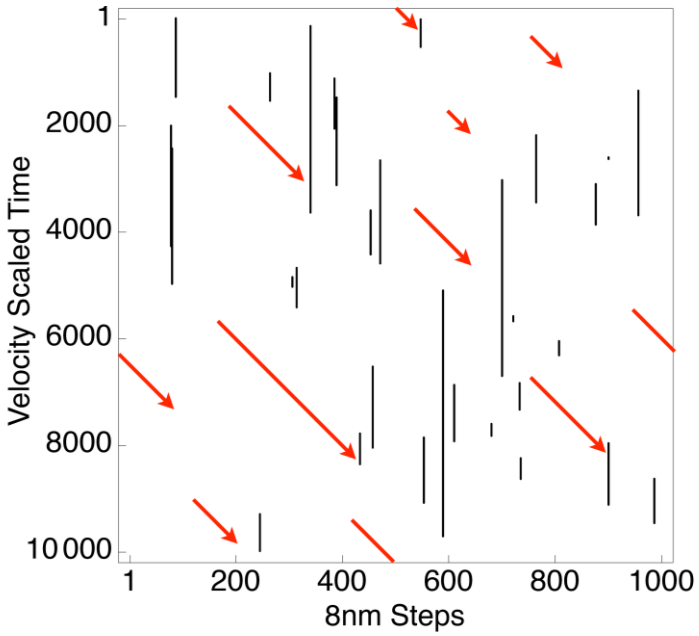

FIGURE S4 Representative simulation of a 3RS-Tau decorated protofilament. Two-dimensional sparse arrays were populated with Tau (vertical black lines) according to the measured 3RS-Tau dwell time and an on-rate that was calibrated with kinesin-1 motility results. The dimensions of the array are scaled such that the size of each bin represents an 8nm step and the amount of time between steps for the appropriate kinesin family member for the x- and y-axes, respectively. Simulated motility is represented by the red arrows, which occur along diagonal elements due to the dimensional scaling. Motility events that reach an edge of the array wrap around to the opposite side due to periodic boundary conditions.

Movie Legends

MOVIE S1 Representative eGFP-kinesin-1 data stepping along rhodamine-labeled paclitaxel microtubules in the absence of Tau. Recorded at 5 frames per second (95 nm / pixel). Playback speed is 10 X the frame rate.

MOVIE S2 Representative eGFP-kinesin-1 data stepping along a single rhodamine-labeled 3RS-Tau decorated paclitaxel microtubule at a 1:5 Tau:tubulin dimer ratio. Recorded at 5 frames per second (95 nm / pixel). Playback speed is 10 X the frame rate.

MOVIE S3 Representative eGFP-kinesin-2 data stepping along rhodamine-labeled paclitaxel microtubules in the absence of Tau. Recorded at 5 frames per second (95 nm / pixel). Playback speed is 10 X the frame rate.

MOVIE S4 Representative eGFP-kinesin-2 data stepping along a single rhodamine-labeled 3RS-Tau decorated paclitaxel microtubule at a 1:5 Tau:tubulin dimer ratio. Recorded at 5 frames per second (95 nm / pixel). Playback speed is 10 X the frame rate.

Supporting References

1. Hinrichs, M. H., A. Jalal, B. Brenner, E. Mandelkow, S. Kumar, and T. Scholz. 2012. Tau protein diffuses along the microtubule lattice. The Journal of biological chemistry 287:38559-38568.
2. McVicker, D. P., G. J. Hoeprich, A. R. Thompson, and C. L. Berger. 2014. Tau interconverts between diffusive and stable populations on the microtubule surface in an isoform and lattice specific manner. Cytoskeleton (Hoboken).
3. Bustamante, C., J. F. Marko, E. D. Siggia, and S. Smith. 1994. Entropic elasticity of lambda-phage DNA. Science 265:1599-1600.
4. Kutys, M. L., J. Fricks, and W. O. Hancock. 2010. Monte Carlo analysis of neck linker extension in kinesin molecular motors. PLoS computational biology 6:e1000980.
5. Sahoo, H., D. Roccatano, M. Zacharias, and W. M. Nau. 2006. Distance distributions of short polypeptides recovered by fluorescence resonance energy transfer in the 10 A domain. Journal of the American Chemical Society 128:8118-8119.
6. Dietz, H., and M. Rief. 2006. Protein structure by mechanical triangulation. Proceedings of the National Academy of Sciences of the United States of America 103:1244-1247.
7. Shastry, S., and W. O. Hancock. 2010. Neck linker length determines the degree of processivity in kinesin-1 and kinesin-2 motors. Current biology : CB 20:939-943.
8. Chretien, D., and R. H. Wade. 1991. New data on the microtubule surface lattice. Biology of the cell / under the auspices of the European Cell Biology Organization 71:161-174.
9. Brunnbauer, M., R. Dombi, T. H. Ho, M. Schliwa, M. Rief, and Z. Okten. 2012. Torque generation of kinesin motors is governed by the stability of the neck domain. Molecular cell 46:147-158.
10. Yajima, J., and R. A. Cross. 2005. A torque component in the kinesin-1 power stroke. Nature chemical biology 1:338-341.
11. Thompson, A. R., G. J. Hoeprich, and C. L. Berger. 2013. Single-molecule motility: statistical analysis and the effects of track length on quantification of processive motion. Biophysical journal 104:2651-2661.